Third-order susceptibility of gold for ultrathin layers

Lysenko, Oleg; Bache, Morten; Lavrinenko, Andrei

Published in:
Optics Letters

Link to article, DOI:
10.1364/OL.41.000317

Publication date:
2016

Document Version
Peer reviewed version

Third-order susceptibility of ultra-thin gold layers

OLEG LYSENKO*, MORTEN BACHE, RADU MALUREANU, AND ANDREI LAVRINENKO

Department of Photonics Engineering, Technical University of Denmark, Oersteds Plads, Building 345V, Kongens Lyngby 2800, Denmark
**Corresponding author: ollyse@fotonik.dtu.dk*

Received XX Month XXXX; revised XX Month, XXXX; accepted XX Month XXXX; posted XX Month XXXX (Doc. ID XXXXX); published XX Month XXXX

This letter presents an experimental study of nonlinear optical effects in stripe plasmonic waveguides. The optical characterization of plasmonic waveguides is performed by a picosecond laser and reveals two nonlinear effects related to propagation of long-range surface plasmon polaritons. The first one is a nonlinear power transmission of plasmonic modes, and the second one is a spectral broadening of plasmonic modes. Both effects depend on the metal layers thickness in plasmonic waveguides, and the experimental values of the third-order susceptibility of the gold layers are obtained. The observed nonlinear effects can be used for future advances in optical communication approaches. © 2015 Optical Society of America

OCIS codes: *(250.5403) Plasmonics; (230.7370) Waveguides; (190.7110) Ultrafast nonlinear optics; (240.6680) Surface plasmons.*

http://dx.doi.org/10.1364/OL.99.099999

Plasmonic waveguides are multilayer structures with unique optical properties. They are utilized in many applications, such as components of integrated optics [1], nanofocusing of electromagnetic radiation [2], and photodetectors [3]. The nonlinear optical effects associated with propagation of a long-range surface plasmon polariton (LRSPP) mode in plasmonic waveguides are investigated less. There are several theoretical approaches to explain the nonlinear properties of metals in plasmonic waveguides. One approach is related to the hydrodynamic model [4], and the cascaded second-order nonlinearity [5]. Another approach is related to the thermo-modulational interband derivative [6]. In the latter case, the third-order susceptibility for bulk gold is derived from the two-temperature model [7]. However, there are less experimental data on the third-order susceptibility in the case of thin metal layers. An overview of some theoretical and experimental results related to the third-order susceptibility of gold has been published recently by R. Boyd and co-workers [8]. In particular, the real part and, partly, the imaginary part of the third-order susceptibility of thin gold layers have been measured by E. Xenogiannopoulou and co-workers using the z-scan method [9].

In this letter the complete third-order susceptibility of thin gold layers is obtained from the experimental study of nonlinear propagation of the LRSPP mode in plasmonic waveguides. The stripe plasmonic waveguides, containing a gold layer, adhesion layers, and silicon dioxide cladding, are fabricated and optically characterized by a high power picosecond laser. The third-order nonlinearities of all constituent materials (metal, adhesion, and cladding) contribute to the effective third-order nonlinearity of a plasmonic mode. Two nonlinear optical effects in the plasmonic waveguides are observed and measured in the experiment. The first effect is the nonlinear transmission and saturation of the output power of the LRSPP mode. The second effect is the spectral broadening of the LRSPP mode. Both effects are measured for several values of the metal thickness. The third-order susceptibility of gold layers is extracted from experimental data, and the obtained results show the effective enhancement of the third-order susceptibility for thinner metal layers.

The samples with plasmonic waveguides are fabricated according to the following steps. Firstly, a photolithography mask is designed in a layout editor, and ordered from a commercial supplier. A silicon wafer with a thick (~6.5 μm) layer of silicon dioxide on top is used as a substrate. A standard ultraviolet lithography process is applied to pattern a photoresist layer. Secondly, a metal layer and adhesion layers are deposited using a sputtering machine. A chemical solution (Piranha) is used to remove the photoresist layer afterwards. An atomic force microscope is used to measure the waveguides profile (Fig. 1a) and metal layers roughness (Fig. 1b). The waveguide profile contains four layers: a bottom adhesion layer (~26 nm), metal layer (~27 nm), top adhesion layer (~26 nm) and small silicon dioxide layer (~21 nm). The layers are deposited one after another in one sputtering program, and the known deposition times and rates are used to calculate the thickness values. The sharp edges on the waveguide profile are the usual artifacts after the lift-off procedure [10]. The roughness profile on the metal surface shows the spikes with the maximum height values ~4 nm. The root mean square (RMS) value for the roughness of the deposited metal layers is ~1.2 nm.

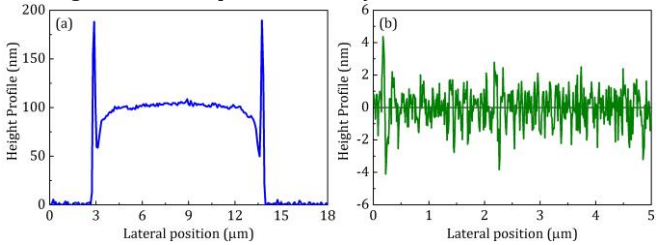

Fig. 1. Atomic force microscope measurements: (a) waveguide profile, and (b) metal layers roughness.

To verify the roughness for the inner layers of the waveguide structure (gold and adhesion), a separate test wafer is prepared. A silicon wafer with a thick (~800 nm) layer of silicon dioxide is used as a substrate. A metal layer and an adhesion layer are deposited on top by

the same procedure, but in different parts of the wafer. A scanning electron microscope is used to image the metal and adhesion surfaces. The gold surface (Fig. 2a) has many bright dots related to the roughness spikes, and the tantalum pentoxide surface (Fig. 2b) is smooth and has no bright dots. The imaging shows that both layers are whole. The metal layer roughness increases the propagation losses of the LRSPP mode in plasmonic waveguides [11]. In this letter we will focus on nonlinear propagation of the LRSPP mode. The metal roughness properties and the fabrication optimization methods will be discussed elsewhere.

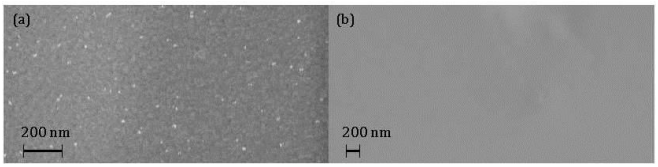

Fig. 2. Scanning electron microscope images: (a) gold surface, and (b) tantalum pentoxide surface.

After the sputtering of waveguides, a cladding layer of silicon dioxide (~5.5 μm) is deposited on top using a standard plasma-enhanced chemical vapor deposition method. The cladding thickness and linear refractive index are measured by a FilmTek 4000. The refractive index value for deposited silicon dioxide is 1.456 at the wavelength 1064 nm. The ready wafer is diced and several samples with the length values 2, 3, and 4 mm are selected for optical characterization. Each sample contains five identical waveguides with the widths 10 μm, and spacing 100 μm. Thus, plasmonic waveguides do not interfere with each other and are independently investigated. Overall, three wafers with the metal layer thicknesses 22, 27, and 35 nm are fabricated by the same procedure and used in the experiment.

The experimental setup to characterize the samples is shown on Fig. 3. The laser source is a picosecond SuperK EXTREME (NKT Photonics) with the average output power in the range 0-15 W, repetition rate 78 MHz, pulse duration ~ 3 ps, and peak wavelength 1064 nm. A free space laser beam is linearly polarized by a polarization controller (Thorlabs), attenuated by a set of neutral density filters, and delivered to the sample by a polarization maintaining fiber. The laser beam polarization is aligned to match the optical axis of the polarization maintaining fiber and to match the transverse magnetic polarization of the LRSPP mode in plasmonic waveguides. A butt coupling method is realized for the excitation of the plamonic modes [12]. A single mode fiber collects and delivers the transmitted optical flux to the optical spectrum analyzer AQ6315E (Yokogawa). The butt coupling alignment is controlled by the optical microscope Axiotech vario (Carl Zeiss). The polarization maintaining fiber is a photonic crystal fiber (NKT Photonics) with the effective mode diameter 8.6 μm. The single mode fiber is a photonic crystal fiber (NKT Photonics) with the mode diameter 8.8 μm. Before the transmission measurements, the LRSPP mode in each waveguide is imaged by a lens (Newport) and a camera beam profiler (Thorlabs), and the transverse magnetic polarization of the plasmonic mode is verified by the polarization controller [13].

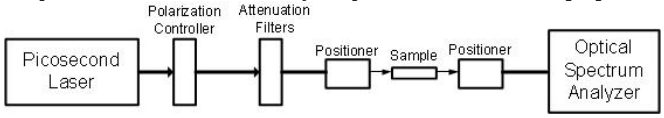

Fig. 3. Experimental setup for nonlinear optical characterization.

Firstly, the linear characterization of the plasmonic waveguides is performed. The laser is tuned to small average power (< 1 mW), and the transmitted power is measured by the optical spectrum analyzer for waveguides with different length values, and the metal thickness values 22, 27, and 35 nm. The insertion loss graphs are used to calculate the propagation loss P per unit length and the coupling loss C per two facets for plasmonic waveguides with the metal thickness values 22, 27, and 35 nm (Fig. 4). For each value of the length and thickness the measurements of five identical waveguides are averaged and the linear fit is calculated by the least squares method. The coupling loss is calculated as the fitted lines cross the ordinates at zero value for the abscissa. The propagation loss is calculated as the slope angle to the fitted lines. The calculated values for P and C, and the calculation errors ε_P and ε_C are presented in Table 1. The obtained experimental values show that the linear propagation loss per unit length increases in ~1.8 times as the gold layer thickness increases from 22 nm to 35 nm. The coupling loss per two facets increases by ~10 %, and does not change within the calculation errors. This conclusion is in accordance with the previous measurements of the similar plasmonic waveguides [14]. The obtained values for P are higher in ~2-3 times than the results published by P. Berini and co-workers, and several possible reasons explain this. Firstly, the maximum values of the roughness spikes of the gold layers are ~4 nm in comparison with ~1 nm in Ref. 14. The obtained RMS value of the metal layers roughness is ~1.2 nm, while the RMS value of the metal layers roughness in Ref. 14 is less than 1 nm. Secondly, the adhesion layers of tantalum pentoxide cause the internal field redistribution in plasmonic waveguides [15], and it also increases the propagation losses in plasmonic waveguides. Meanwhile the nonlinear properties of tantalum pentoxide are well-known [16], and its use provides less propagation losses in plasmonic waveguides than the use of metallic adhesion materials, such as titanium [17]. The sharp edges on the waveguide profile on Fig. 1a do not contribute to the propagation losses as the field intensity of the LRSPP mode is close to zero at the waveguide corners [18]. The peak wavelength 1550 nm used in Ref. 14 also provides lower attenuation of the LRSPP mode in plasmonic waveguides than the peak wavelength 1064 nm [18].

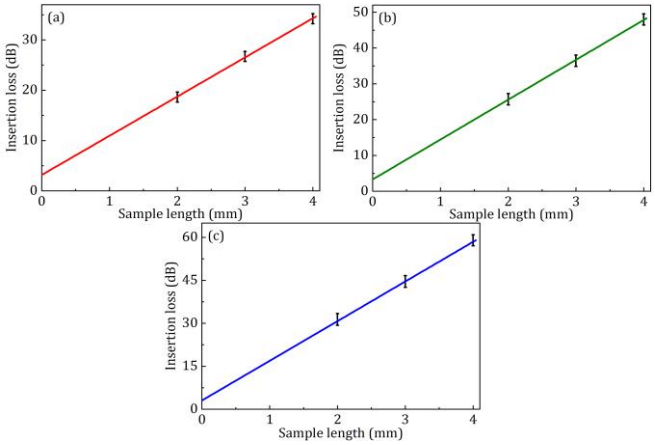

Fig. 4. Propagation loss and coupling loss measurements of plasmonic waveguides with the gold layer thickness (a) t = 22 nm, (b) t = 27 nm, and (c) t = 35 nm.

Table 1. Experimental values of the propagation loss and coupling loss for plasmonic waveguides with the gold layer thicknesses 22, 27, and 35 nm.

t (nm)	P (dB/mm)	ε_P (dB/mm)	C (dB)	ε_C (dB)
22	7.79	0.17	3.16	0.52
27	11.14	0.24	3.29	0.75
35	13.83	0.33	3.49	1.02

Secondly, the nonlinear characterization of the plasmonic waveguides is performed. The laser current is increased, and the average power delivered to the waveguides is tuned in the range 0-480 mW by turning the attenuation filters. The transmitted power is measured by the optical spectrum analyzer for plasmonic waveguides with the length 3 mm, and the metal thickness values 22, 27, and 35 nm. The obtained dependencies of the transmitted power P_{out} with respect to the delivered power P_{in} have several interesting features (Fig. 5). The first feature is the nonlinear trends of the dependencies $P_{out}(P_{in})$ at high values of the input power P_{in}. The second feature is that these nonlinear trends depend on the metal layers thickness t in plasmonic waveguides. The plasmonic waveguides with thinner metal layers have more pronounced deviation from the linear power dependences at the same values of the input power. For each value of the metal thickness the measurements of five identical waveguides are averaged and the nonlinear curve fit is calculated as follows:

$$P_{out} = aP_{in} - bP_{in}^{2}, \qquad (1)$$

where a and b are the experimental coefficients. The calculated values for a and b, and calculation errors ε_a, ε_b are presented in Table 2. Coefficient a corresponds to the linear propagation regime of the LRSPP mode. The value of a for the metal thickness t = 35 nm is in ~350 times less than for the metal thickness t = 22 nm. This is expected as the thick metal layers cause higher losses for the propagation of the plasmonic mode. The coefficient b is related to nonlinear properties of the plasmonic mode. The nonlinearities of the constituent materials (metal, adhesion, and cladding) in plasmonic waveguides contribute to the effective nonlinearity of the LRSPP mode and lead to the observed nonlinear behavior.

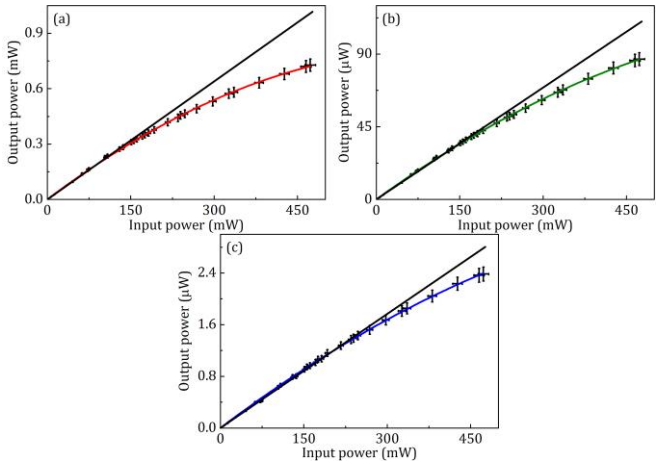

Fig. 5. Nonlinear power transmission for plasmonic waveguides with the gold layer thickness (a) t = 22 nm, (b) t = 27 nm, and (c) t = 35 nm. Black lines on each graph correspond to linear propagation of the LRSPP mode.

Table 2. Experimental values of the coefficients a and b for plasmonic waveguides with the gold layer thicknesses 22, 27, and 35 nm.

t (nm)	a	ε_a	b (1/W)	ε_b (1/W)
22	$2.26 \cdot 10^{-3}$	$0.01 \cdot 10^{-3}$	$1.54 \cdot 10^{-3}$	$0.02 \cdot 10^{-3}$
27	$2.49 \cdot 10^{-4}$	$0.01 \cdot 10^{-4}$	$1.38 \cdot 10^{-4}$	$0.02 \cdot 10^{-4}$
35	$6.53 \cdot 10^{-6}$	$0.03 \cdot 10^{-6}$	$3.09 \cdot 10^{-6}$	$0.08 \cdot 10^{-6}$

In terms of the nonlinear response of the constituent materials, gold has dominant contribution in the effective third-order susceptibility $\chi^{(3)}$ of the plasmonic mode [19]. The effective third-order susceptibility of the LRSPP mode in plasmonic waveguides is related to the nonlinear absorption coefficient β as follows [20]:

$$\beta = \frac{2\omega}{c}\frac{\mathrm{Im}[n_2]}{A}, \qquad n_2 = \frac{3}{4\varepsilon_0 c n_0 \,\mathrm{Re}[n_0]}\chi^{(3)}. \qquad (2)$$

Here $\omega = 2\pi c/\lambda$ is the light angular frequency, c is the speed of light in vacuum, ε_0 is the vacuum permittivity, n_0 and n_2 are the effective linear and nonlinear refractive indices of the LRSPP mode, and A is the effective area of the LRSPP mode. The nonlinear coefficient b depends on both the nonlinear parameters of the LRSPP mode and the laser parameters. By considering the pulse propagation equation [15], it is straightforward to show that the ratio $b/a \approx \beta/(\alpha_0 T\nu)$, where α_0 is the linear attenuation coefficient of the LRSPP mode, T is the laser pulse duration, and ν is the laser repetition rate. In the case of plasmonic waveguides the direct proportionality $\beta \sim \mathrm{Im}[\chi_f^{(3)}]$ is realized, and the obtained coefficients a and b are used to extract the imaginary part of the third-order susceptibility of the gold layers.

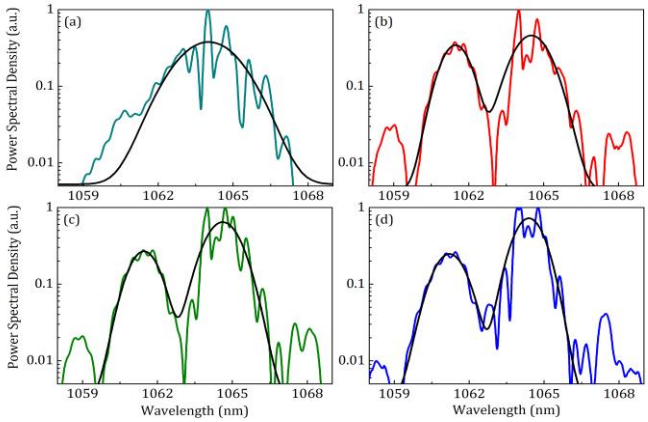

Fig. 6. (a) Input pulse spectrum, and output pulse spectra for plasmonic waveguides with the gold layer thickness (b) t = 22 nm, (c) t = 27 nm, and (d) t = 35 nm. Black lines on each graph correspond to Gaussian curves fit to the measured spectra.

The spectra of the transmitted optical flux are measured as well by the optical spectrum analyzer in the wavelength range 1058-1069 nm, and have several interesting features (Fig. 6). The first feature is splitting of the input pulse into several output pulses. The Gaussian curves fit to the measured spectra shows at least two big optical pulses separated in the output spectra. The second feature is that the pulses broadening and splitting in the output spectra differs slightly for plasmonic waveguides with the metal layer thicknesses 22, 27, and 35 nm. The quantitative analysis is done by comparing the values of the effective spectral widths for the input pulse and output pulses at the splitting level (~ 0.05). The spectral broadening factor (SBF), and the effective nonlinear coefficient γ are given by [21]:

$$\mathrm{SBF} \approx 0.86\gamma P_0 \frac{1-e^{-\alpha_0 L}}{\alpha_0}, \qquad \gamma = \frac{\omega}{c}\frac{\mathrm{Re}[n_2]}{A}, \qquad (3)$$

where P_0 is the peak power of an input pulse, and L is the length of a plasmonic waveguide. The direct proportionality $\gamma \sim \mathrm{Re}[\chi_f^{(3)}]$ is also

realized, and the experimental values of the SBF are used to extract the real part of the third-order susceptibility of a gold layer.

The calculated values of the real and imaginary parts of the third-order susceptibility $\chi_f^{(3)}$ of the gold layers with different thicknesses, and the calculation errors are presented in Table 3. Both the real and imaginary parts of the third-order susceptibility decrease as the layer thickness increases. For comparison with the theoretical value of the third-order susceptibility for bulk gold $\chi_\infty^{(3)} = (4.56 + i \cdot 0.48) \cdot 10^{-18}$ m^2/V^2 [7] the experimental values for the third-order susceptibility $\chi_f^{(3)}$ are plotted (Fig. 7) and the nonlinear curve fit is calculated as follows [15]:

$$\chi_f^{(3)} = \chi_\infty^{(3)} + \frac{C}{t}, \quad (4)$$

where t is the gold layer thickness, and C is the experimental coefficient. The calculated values for the real part of the experimental coefficient $\mathrm{Re}[C] = (5.82 \pm 0.15) \cdot 10^{-24}$ m^3/V^2, and the imaginary part of the experimental coefficient $\mathrm{Im}[C] = (9.34 \pm 1.79) \cdot 10^{-26}$ m^3/V^2.

The obtained results have several interesting features. The experimental values of the real part of $\chi_f^{(3)}$ are in ~4-5 times higher than the asymptote value of the real part of $\chi_\infty^{(3)}$ for bulk gold. The experimental values of the imaginary part of $\chi_f^{(3)}$ are in ~1.5-2 times higher than the asymptote value of the imaginary part of $\chi_\infty^{(3)}$ for bulk gold. Figure 7 also indicates the thickness limitations for the experimental determination of the third-order susceptibility. The Drude model stops working at the gold layer thicknesses below 10-15 nm due to the layer clustering process [22]. On the other side, the LRSPP mode breaks down at the gold layers thicknesses above 50-60 nm due to the small penetration depth of the electromagnetic field in metal [18]. Thus, the possible thickness values for determination of the third-order susceptibility of metal layers are in the range ~15–45 nm.

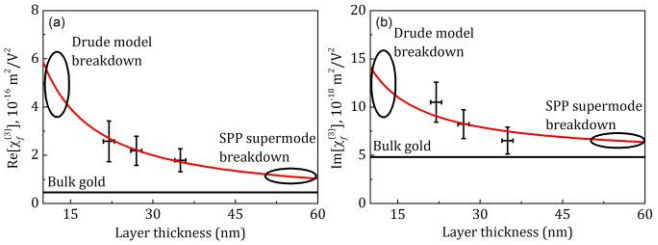

Fig. 7. (a) Real part and (b) imaginary part of the third-order susceptibility of gold layers with the thicknesses 22, 27, and 35 nm. Red curves show the nonlinear curve fit to experimental data, black lines show the third-order susceptibility values for bulk gold

Table 3. Experimental values of the third-order susceptibility $\chi_f^{(3)}$ of gold layers with different thicknesses.

t (nm)	$\mathrm{Re}[\chi_f^{(3)}]$ (m^2/V^2)	$\varepsilon_{\mathrm{Re}[\chi_f^{(3)}]}$ (m^2/V^2)	$\mathrm{Im}[\chi_f^{(3)}]$ (m^2/V^2)	$\varepsilon_{\mathrm{Im}[\chi_f^{(3)}]}$ (m^2/V^2)
22	$2.57 \cdot 10^{-16}$	$0.84 \cdot 10^{-16}$	$10.5 \cdot 10^{-18}$	$2.08 \cdot 10^{-18}$
27	$2.18 \cdot 10^{-16}$	$0.61 \cdot 10^{-16}$	$8.22 \cdot 10^{-18}$	$1.49 \cdot 10^{-18}$
35	$1.79 \cdot 10^{-16}$	$0.48 \cdot 10^{-16}$	$6.51 \cdot 10^{-18}$	$1.38 \cdot 10^{-18}$

There are several possible reasons to explain the increase of the third-order susceptibility in gold layers. Firstly, the effective enhancement of the third-order nonlinearity in a metal layer can be caused by the change in the free electrons motion. The electrons in a metal layer start to feel the borders, their collisions frequency increases, it leads to the effective increase of the dielectric permittivity of a metal layer, which in turn causes the increase of the third-order susceptibility of a metal layer. Secondly, by considering the ultra-fast electrons dynamics in metal [7], it is possible to assume that, for the electrons heated by a laser pulse, the effective thermalization rates with other electrons and the metal lattice change in the case of a metal layer. These thermalization rates depend on the layer thickness, and it causes effective enhancement of the third-order susceptibility in a metal layer.

The obtained dependencies of the third-order susceptibility for the gold layers are in accordance with previous measurements of thin gold layers using the z-scan method [9]. The presented nonlinear optical effects in plasmonic waveguides can be used for the development of future optical communication systems. For example, the idea of spectral broadening in plasmonic waveguides can be realized in the design of a compact on-chip frequency converter.

Acknowledgment. The authors thank G. Wurtz and A. Zayats from King's College London for the valuable comments regarding the fabrication process and the fruitful discussions.

References

1. A. Maradudin, J. Sambles, W. Barnes, *Modern Plasmonics* (Elsevier, 2014).
2. D. Gramotnev and S. Bozhevolnyi, Nat. Photonics 8, 13 (2014).
3. P. Berini, Laser Photon. Rev. 8, 2, 197 (2014).
4. M. Scalora, M. Vincenti, D. de Ceglia, V. Roppo, M. Centini, N. Akozbek, and M. Bloemer, Phys. Rev. A 82, 043828 (2010).
5. P. Ginzburg, A. Krasavin, and A. Zayats, New J. Phys. 15, 013031 (2013).
6. M. Conforti and G. Della Valle, Phys. Rev. B 85, 245423 (2012).
7. A. Marini, M. Conforti, G. Della Valle, H. W. Lee, Tr. X. Tran, W. Chang, M. A. Schmidt, S. Longhi, P. St. J. Russell, and F. Biancalana, New J. Phys. 15, 013033 (2013).
8. R. Boyd, Z. Shi, and I. De Leon, Opt. Commun. 326, 74 (2014).
9. E. Xenogiannopoulou, P. Aloukos, S. Couris, E. Kaminska, A. Piotrowska, and E. Dynowska, Opt. Commun. 275, 217 (2007).
10. O. Geschke, H. Klank, and P. Telleman, *Microsystem Engineering of Lab-on-a-Chip Devices* (Wiley, 2004).
11. A. Maradudin, *Light Scattering and Nanoscale Surface Roughness* (Springer, 2007).
12. R. Hunsperger, *Integrated Optics: Theory and Technology* (Springer, 2002).
13. R. Charbonneau, P. Berini, E. Berolo, and E. Lisicka-Shrzek, Opt. Lett. 25, 11, 844 (2000).
14. P. Berini, R. Charbonneau, N. Lahoud, and G. Mattiussi, J. Appl. Phys. 98, 043109 (2005).
15. O. Lysenko, M. Bache, and A. Lavrinenko, "Nonlinear optical model for plasmonic waveguides" http://www.arxiv.org.
16. C. Tai, J. S. Wilkinson, N. M. B. Perney, M. Caterina Netti, F. Cattaneo, C. E. Finlayson, and J. J. Baumberg, Opt. Express 12, 21, 5110 (2004).
17. T. G. Habteyes, S. Dhuey, E. Wood, D. Gargas, S. Cabrini, P. J. Schuck, P. Alivisatos, and S. R. Leone, ACSNANO 6, 6, 5702 (2012).
18. S. Maier, *Plasmonics: Fundamentals and Applications* (Springer, 2007).
19. A. Baron, S. Larouche, D. J. Gauthier, and D. R. Smith, J. Opt. Soc. Am. B 32, 1, (2015).
20. R. Boyd, *Nonlinear Optics* (Academic Press, 2008).
21. G. Agrawal, *Nonlinear Fiber Optics* (Academic Press, 2007).
22. U. Kreibig and M. Vollmer, *Optical Properties of Metal Clusters* (Springer, 1995).

Full references

1. A. Maradudin, J. Sambles, W. Barnes, *Modern Plasmonics* (first edition, Elsevier, 2014).

2. D. Gramotnev and S. Bozhevolnyi, "Nanofocusing of electromagnetic radiation", Nat. Photonics 8, 13-22 (2014).

3. P. Berini, "Surface plasmon photodetectors and their applications", Laser Photon. Rev. 8, 2, 197–220 (2014).

4. M. Scalora, M. A. Vincenti, D. de Ceglia, V. Roppo, M. Centini, N. Akozbek, and M. J. Bloemer, "Second- and third-harmonic generation in metal-based structures", Phys. Rev. A 82, 043828, 1-14 (2010).

5. P. Ginzburg, A. Krasavin, and A. Zayats, "Cascaded second-order surface plasmon solitons due to intrinsic metal nonlinearity", New J. Phys. 15, 013031 (2013).

6. M. Conforti and G. Della Valle, "Derivation of third-order nonlinear susceptibility of thin metal films as a delayed optical response", Phys. Rev. B 85, 245423 (2012).

7. A. Marini, M. Conforti, G. Della Valle, H. W. Lee, Tr. X. Tran, W. Chang, M. A. Schmidt, S. Longhi, P. St. J. Russell, and F. Biancalana, "Ultrafast nonlinear dynamics of surface plasmon polaritons in gold nanowires due to the intrinsic nonlinearity of metals", New J. Phys. 15 013033 (2013).

8. R. Boyd, Z. Shi, and I. De Leon, "The third-order nonlinear optical susceptibility of gold", Opt. Commun. 326, 74-79 (2014).

9. E. Xenogiannopoulou, P. Aloukos, S. Couris, E. Kaminska, A. Piotrowska, and E. Dynowska, "Third-order nonlinear optical properties of thin sputtered gold films", Opt. Commun. 275, 217-222 (2007).

10. O. Geschke, H. Klank, and P. Telleman, *Microsystem Engineering of Lab-on-a-Chip Devices*, (second edition, Wiley, 2004).

11. A. Maradudin, *Light Scattering and Nanoscale Surface Roughness* (Springer, 2007).

12. R. Hunsperger, *Integrated Optics: Theory and Technology* (fifth edition, Springer, 2002).

13. R. Charbonneau, P. Berini, E. Berolo and E. Lisicka-Shrzek, "Experimental observation of plasmon–polariton waves supported by a thin metal film of finite width," Opt. Lett. 25, 11, 844-846 (2000).

14. P. Berini, R. Charbonneau, N. Lahoud and G. Mattiussi, "Characterization of long-range surface-plasmon-polariton waveguides," J. Appl. Phys. 98, 043109 (2005).

15. O. Lysenko, M. Bache, and A. Lavrinenko, "Nonlinear optical model for plasmonic waveguides", http://www.arxiv.org.

16. C. Tai, J. S. Wilkinson, N. M. B. Perney, M. Caterina Netti, F. Cattaneo, C. E. Finlayson, and J. J. Baumberg, "Determination of nonlinear refractive index in a Ta2O5 rib waveguide using self-phase modulation", Opt. Express, 12, 21, 5110 (2004).

17. T. G. Habteyes, S. Dhuey, E. Wood, D. Gargas, S. Cabrini, P. J. Schuck, P. Alivisatos, and S. R. Leone, "Metallic Adhesion Layer Induced Plasmon Damping and Molecular Linker as a Nondamping Alternative", ACSNANO, 6, 6, 5702-5709 (2012).

18. S. Maier, *Plasmonics: Fundamentals and Applications* (Springer, 2007).

19. A. Baron, S. Larouche, D. J. Gauthier, and D. R. Smith, "Scaling of the nonlinear response of the surface plasmon polariton at a metal/dielectric interface", J. Opt. Soc. Am. B 32, 1 (2015).

20. R. Boyd, *Nonlinear Optics* (third edition, Academic Press, 2008).

21. G. Agrawal, *Nonlinear Fiber Optics* (fourth edition, Academic Press, 2007).

22. U. Kreibig, M. Vollmer, *Optical Properties of Metal Clusters* (Springer, 1995).